



## Preparation of starch sulfate resin and its adsorption performance for malachite green

Lei Guo<sup>a,\*</sup>, Yuanchao Cao<sup>a</sup>, Guiying Li<sup>a</sup>, Junshen Liu<sup>a</sup>, Ling Han<sup>b</sup>, Hanlin Zhang<sup>c</sup>

<sup>a</sup>School of Chemistry and Materials Science, Ludong University, Yantai 264025, China, Tel. +86 535 6672176; Fax: +86 535 6696162; email: unikguo@gmail.com (L. Guo), Tel. +86 535 6672176; emails: 1076197425@qq.com (Y. Cao), 26362442@qq.com (G. Li), xincailhuanbao@qq.com (J. Liu)

<sup>b</sup>Wanhua Energysav Science & Technology Group Co., Ltd., Yantai 264013, China, Tel. +86 535 3387397, email: hanling@whchem.com

<sup>c</sup>Qingdao Entry-Exit Inspection and Quarantine Bureau, Qingdao 266001, China, Tel. +86 532 80887303; email: 45880080@qq.com

Received 26 June 2017; Accepted 15 November 2017

### ABSTRACT

Starch sulfate resin (SSR) was prepared in the form of spherical beads by an emulsion crosslinking technique and used to adsorb malachite green (MG) from aqueous solution. The effects of time, concentration of MG, temperature, and pH were investigated via static adsorption experiments. The adsorption processes reach equilibrium in about 60 min, and the kinetic data conform to the pseudo-first-order model. The adsorption equilibrium data are well described by the Langmuir isotherm model with a maximum adsorption capacity of 173.92 mg/g at 288 K. The result of thermodynamic studies indicates that the adsorption process is spontaneous and endothermic. The adsorption capacities of MG on SSR first increase and then decrease with the pH increasing from 2.0 to 10.0, and the optimal adsorption performance is achieved at pH = 6.0. The dynamic adsorption performance of MG on SSR was also investigated. The adsorption capacity decreases after five cycles of adsorption and desorption process; however, the adsorbent still has a promising potential on the adsorption of MG.

*Keywords:* Starch sulfate resin; Malachite green; Column adsorption; Emulsion crosslinking

### 1. Introduction

Environmental issues have attracted considerable attention of humans for years. The pollution caused by synthetic dyes has threatened our health and ecological balance, since many kinds of dyes are used in different fields, such as food, leather, textile, garment industry and so on. Many dyes are toxic and released into the environment without adequate treatment because of the limits of economy and technology. Malachite green (MG), one kind of cationic dyes, has been used to control parasites in fish or fish eggs, fungal or bacterial infections [1]. The effectiveness of MG is remarkable, but it is toxic, high persistence, carcinogenic, mutagenic and causes other side effects [2]. Therefore, it is urgent to remove it from the aqueous system before being adversely affected.

A variety of methods to remove the dyes from the wastewater have been reported, such as photocatalysis [3], adsorption [4], biodegradation [5], and coagulation [6]. Among these technologies, adsorption is favored by researchers due to its low cost, efficiency, easy operation, and no secondary pollution. Many materials, such as clayey soil [7], chitin hydrogels [8], melamine/maleic anhydride sorbent [9], multi-walled carbon nanotubes [10], and walnut shell [11], have been studied as the adsorbents of MG.

Starch is a kind of abundant natural polysaccharide, playing a great role in our daily life. Starch is stored in the plant that can be extracted from corn, sweet potato, wild acorns. As an adsorbent, starch derivatives show many promising properties such as environmentally friendly material, high adsorption capacity, and biodegradation [12].

In our work, we prepared the SSR in the form of spherical beads by an emulsion crosslinking technique. The spherical bead shape makes SSR feasible to be used as the filler

\* Corresponding author.

of adsorption column and easy to be separated after static adsorption. We investigated the potential of the SSR to remove MG from aqueous solution. The effects of contact time, MG concentration, temperature, and pH values on the adsorption were well studied via static adsorption experiments, and the reusability of SSR was also investigated via dynamic adsorption experiments.

## 2. Materials and methods

### 2.1. Materials

Corn starch, purchased from Zhucheng Xingmao Corn Developing Co., Ltd., China, was dried at 105°C before it was used. Sodium nitrite, sodium bisulfite, paraffin oil, and glycol were purchased from Sinopharm Reagent chemicals Co., Ltd, China. Epichlorohydrin was purchased from Tianjin Bodi Chemical Co., Ltd. MG was obtained from Tianjin Fuchen Chemical Reagents Factory (Tianjin, China). Span 20 and ethanol were purchased from Tianjin Damao Chemical Reagents Factory (Tianjin, China). All of the reagents are analytic reagent grade and used without further purification. All solutions and standards were prepared by using distilled water.

### 2.2. Preparation of SSR

Starch sulfate was prepared according to the method described in previous work [13].

An emulsion crosslinking technique was used to prepare SSR. A pre-weighed amount of starch sulfate and sodium hydroxide was dissolved in distilled water (8 mL) in the beaker. The mixture was heated in the boiling water until completely dissolved. After cooling the solution down to the ambient temperature, glycol (0.62 g) and epichlorohydrin (2.31 g) were added. Liquid paraffin (24 mL) and span 20 (0.48 g) were placed into a three-necked flask and evenly mixed. The starch mixture was added into the flask and stirred to form water-in-oil droplets. The emulsion crosslinking reaction proceeded for 3 h at 80°C. The resultant spherical resin was filtered off and Soxhlet extracted with ethanol:water (7:3, V/V) for 24 h. SSR was dried at 60°C in a vacuum oven for 24 h and sieved to collect the 20–60 mesh size fractions.

### 2.3. Characterization methods

The sulfur contents of starch sulfate and SSR were determined by inductively coupled plasma atomic emission spectrometer (ICP-AES) (ICPE 9000, Japan). The structures of SSR were analyzed by using a Fourier-transform infrared spectrometer (Tensor 37, German). The morphology was obtained by an optical microscope (XSP-06-1600X, China) and a scanning electron microscope (SEM, JEOL JSM-5610 LV, Japan).

The equilibrium swelling degree (ESD) of SSR was determined by swelling 0.5 g dried SSR in 10 mL distilled water, overnight in a measuring cylinder. The ESD (mL/mL) was expressed as the ratio of the swollen volume to the volume of dried microspheres.

The water absorption (WA) of SSR was determined as follows. A pre-weighed amount of SSR was immersed in excess distilled water until swelling equilibrium was reached. Then the swollen SSR was taken out, and the excess water was

removed by filtering through the 100-mesh sieve. The weight of the swollen SSR was measured. The WA could be defined as follows:

$$\text{WA (\%)} = (W_1 - W_0) / W_0 \times 100 \quad (1)$$

where  $W_0$  is the initial weight of SSR before immersion in water, and  $W_1$  is the weight of swollen SSR.

### 2.4. Adsorption experiments

#### 2.4.1. Static adsorption experiments

Static adsorption experiments were conducted in a series of 100 mL glass stopper Erlenmeyer flasks containing 50 mL MG solution and 50 mg adsorbent. The mixture was oscillated on a water bath oscillator on a uniform speed at a set temperature. After a certain adsorption time, the supernatant of the solution was centrifuged at high speed, taking the supernatant and measuring its absorbance using a VIS spectrophotometer (VIS-721, Yoke Instrument, China) at the maximum wavelength of 617 nm. The adsorption capacity for MG was calculated according to the standard curve.

The adsorption capacity of MG on SSR was calculated according to the following equation:

$$Q = \frac{(C_i - C_f)}{m} V, \quad (2)$$

where  $Q$  (mg/g) is the adsorption capacity of MG on SSR,  $C_i$  and  $C_f$  (mg/L) represent the initial and terminal concentrations of MG, respectively,  $V$  (L) is the volume of MG solution, and  $m$  (g) is the mass of the adsorbent.

#### 2.4.2. Dynamic adsorption experiments

We investigated the reusability of the adsorbent in five consecutive adsorption and desorption cycles. The experiment was carried out as follows: pump the MG solution (300 mg/L) at a constant speed into the fix-bed column ( $\Phi = 1.5$  cm) equipped with 10 cm height of adsorbent (1.24 g) until saturated. During the process, determine the absorbance of the solution per 5 min upon the first drop falling. When the column was saturated, pump the hydrochloric acid (1 mol/L) at a constant speed into the adsorption column. The absorbance of the eluent was measured per 1 min as described above. The process would not stop until it was completely eluted. Repeat the process for five times. Before every adsorption and desorption cycle, the column was eluted with distilled water until reaching a constant pH.

Every adsorption experiments were repeated three times. The relative errors of the repeated experiments' results were all less than 3.0%.

## 3. Results and discussion

### 3.1. Characterization of SSR

The sulfur contents of starch sulfate and SSR are 5.06 and 2.39 mmol/g, respectively. The IR spectra of the native corn starch and SSR are shown in Fig. 1. Bands resulting from S=O stretching at 1,206  $\text{cm}^{-1}$ , S–O stretching at 876  $\text{cm}^{-1}$ , C–O–C

stretching at  $1,114\text{ cm}^{-1}$ , and C–Cl stretching at  $621\text{ cm}^{-1}$  can be observed in the spectrum of SSR. These bands can prove that the product is starch sulfate resin.

The morphology of SSR under an optical microscope is also shown in Fig. 1. SSR is in the form of spherical beads with an irregular surface under a  $250\times$  magnification. The diameter of the spherical beads in Fig. 1 is about  $0.62\text{ mm}$ . The morphology of SSR under SEM is shown in Fig. 2. It can also be seen that the beads with a diameter of about  $0.60\text{ mm}$  have the irregular surface.

Before the adsorption experiments, we investigated the ESD and the WA of the adsorbent. The ESD and WA of SSR were  $4.8\text{ mL/mL}$  and  $385\%$ , respectively. The high values

of ESD and WA mean good hydrophilicity and potential adsorption capacity of SSR.

### 3.2. Adsorption kinetics of MG on SSR

The adsorption kinetics mainly studies on the adsorption rate of the adsorbent. Fig. 3 shows the relationship between adsorption capacity of MG on SSR and contact time. The adsorption capacity increases with the increase of contact time in the first  $60\text{ min}$ , and then the adsorption reaches equilibrium. As a cationic dye, MG can be adsorbed on SSR mainly due to the negative sulfate groups of SSR. The adsorption at the beginning is fast because more sulfate groups are available to adsorb MG. With the extension of time, the active sulfate groups gradually decrease, and the adsorption eventually reaches equilibrium.

In order to understand the adsorption mechanism of MG on SSR, the pseudo-first-order [14] and the pseudo-second-order kinetic models [15] were used to test the experimental data. The two kinetic models are generally written as follows:

$$Q = Q_e(1 - e^{-K_1 t}), \quad (3)$$

$$Q = \frac{K_2 Q_e^2 t}{1 + K_2 Q_e t}, \quad (4)$$

where  $Q$  and  $Q_e$  (mg/g) are the adsorption capacities at time  $t$  (min) and equilibrium, respectively;  $K_1$  (1/min) and  $K_2$  (g/(mg min)) represent the pseudo-first-order and pseudo-second-order kinetic rate constants, respectively.

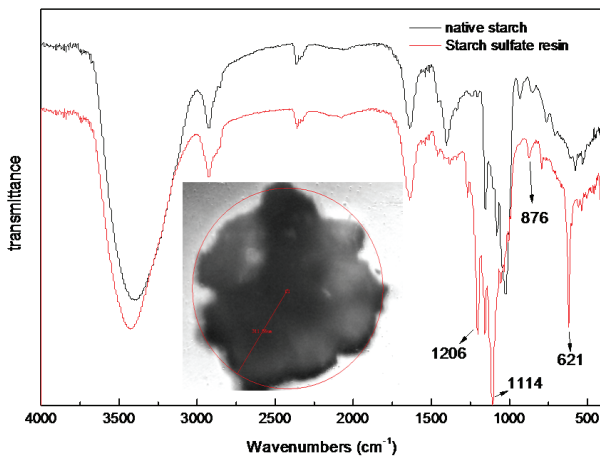


Fig. 1. IR spectra and the morphology of SSR.

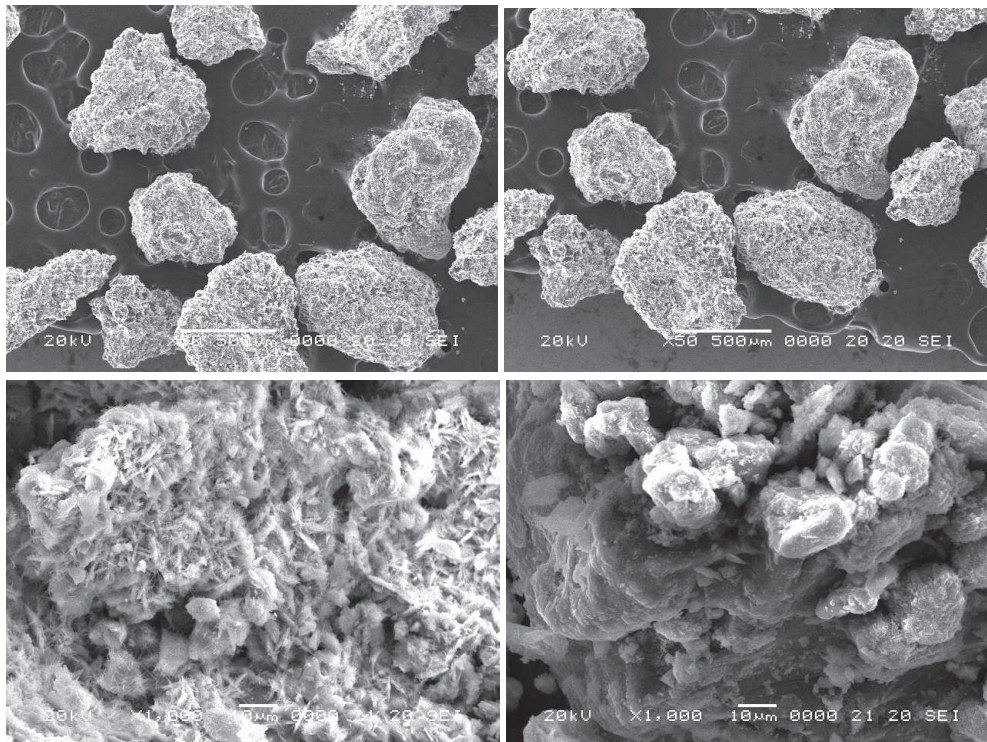


Fig. 2. SEM photographs of SSR.

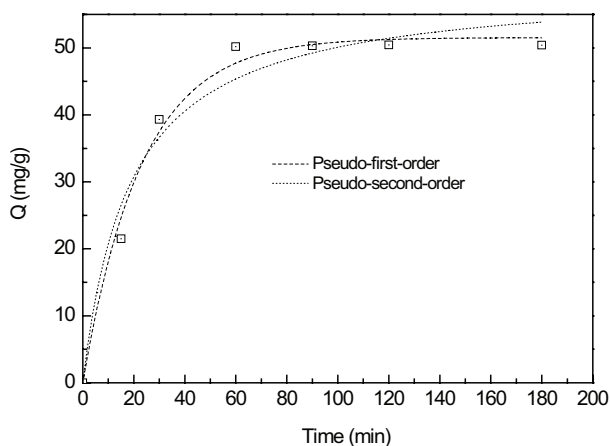


Fig. 3. Effect of the adsorption time on the adsorption capacities of MG at 288 K and the kinetic fitting curves.

The nonlinear regression analysis method was used to fit the kinetic models, as shown in Fig. 3. The parameters of the two kinetic models are summarized in Table 1.

Fig. 3 shows that the pseudo-first-order kinetic model better fitted the data with a higher correlation coefficient ( $0.9912 > 0.9703$ ) than the pseudo-second-order kinetic model. The value of  $Q_e$  from the pseudo-first-order kinetic model fitting is closer to the corresponding experimental  $Q$  value. So the adsorption kinetics of MG on SSR can be well described with pseudo-first-order kinetic model. Wang and Ariyanto [16] used natural zeolite to remove MG and  $Pb^{2+}$  ions from aqueous solution, and the result also followed the pseudo-first-order kinetic model. In all the following experiments, the adsorption time was 60 min.

### 3.3. Adsorption equilibrium isotherm of MG on SSR

Adsorption equilibrium expresses the relationship between the equilibrium concentration and equilibrium adsorption capacity at a certain temperature. The effect of MG equilibrium concentration on the equilibrium adsorption capacity is shown in Fig. 4. The adsorption capacities increase rapidly with the increase of the equilibrium concentration at the beginning. The initial MG concentration provides a powerful driving force to overcome the resistance to the mass transfer of MG between the aqueous solution and solid phase [10]. With the increase of MG concentration, the adsorption reaches equilibrium, and SSR becomes saturated. Furthermore, we can see from the curves that the maximum of equilibrium adsorption capacities increased with the increase of temperature.

Langmuir [17], Freundlich [18], and Sips [19] models were used to analyze the experimental data with the aim to determine the adsorption mechanism. The equations of the three models are expressed in Table 2. The nonlinear fitting curves and parameters are shown in Fig. 4 and Table 3, respectively. According to the  $R^2$  values, the Langmuir model ( $R^2 > 0.99$ ) fits the adsorption data very well, which indicates that the adsorption of MG on SSR is likely to be a monolayer adsorption and the active sites distributed on the surface are homogeneous [20]. Bulut et al. [21] investigated the adsorption of MG on bentonite and found that the Langmuir isotherm suited the experimental data best. The data also suits

Table 1  
Kinetic model parameters for the adsorption of MG on SSR

Kinetic models	Parameters	Values
Pseudo-first-order	$Q_e$ (mg/g)	51.53
	$K_1$ (1/min)	0.043
	$R^2$	0.9912
Pseudo-second-order	$Q_e$ (mg/g)	59.40
	$K_2$ (g/(mg min))	$9.06 \times 10^{-4}$
	$R^2$	0.9703
Experimental data	$Q_e$ (mg/g)	50.43

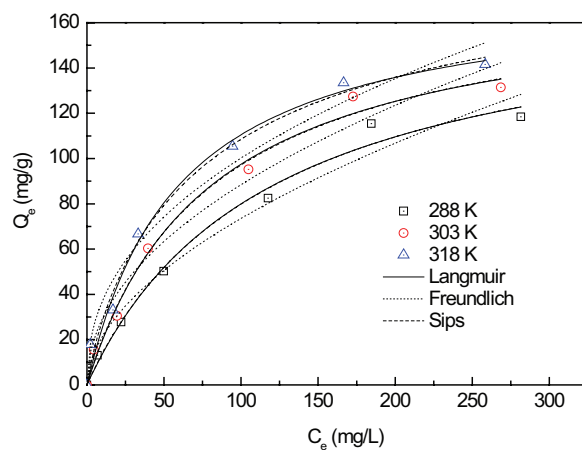


Fig. 4. Effect of the equilibrium MG concentration on the adsorption capacities and adsorption equilibrium isotherms.

Table 2  
The summary of adsorption isotherms

Isotherm	Equation	Parameters
Langmuir	$Q_e = \frac{Q_m K_L C_e}{1 + K_L C_e}$	$K_L$ : the Langmuir equilibrium constant related to adsorption affinity, L/mg
Freundlich	$Q_e = K_F C_e^{1/n}$	$K_F$ : the Freundlich constant related to the adsorption capacity, (mg/g)(L/mg) $^{1/n}$ ; $n$ , the Freundlich constant related to adsorption intensity
Sips	$Q_e = \frac{Q_m (K_s C_e)^{1/s}}{1 + (K_s C_e)^{1/s}}$	$K_s$ : the Sips equilibrium constant related to adsorption affinity, L/mg; $s$ : the heterogeneity factor

the Sips model well. This model combines the Langmuir and Freundlich isotherm type models [22].

### 3.4. Adsorption thermodynamic studies

The extent and driving force of the adsorption process can be understood through the adsorption thermodynamics.  $K_L$  (L/mg) in Langmuir isotherm represents the adsorption

Table 3  
The isotherm parameters for the adsorptions of MG on SSR

Isotherms	Parameters	Temperature		
		288 K	303 K	318 K
Langmuir	$Q_m$ (mg/g)	173.92	175.00	176.26
	$K_L$ (L/mg)	$8.52 \times 10^{-3}$	$1.26 \times 10^{-2}$	$1.68 \times 10^{-2}$
	$R^2$	0.9904	0.9963	0.9909
Freundlich	$K_f$ ((mg/g) (L/mg) <sup>1/n</sup> )	6.18	9.66	13.64
	$N$	1.86	2.08	2.31
	$R^2$	0.9776	0.9758	0.9786
Sips	$Q_m$ (mg/g)	176.05	178.52	195.58
	$K_s$ (L/mg)	$8.28 \times 10^{-3}$	$1.20 \times 10^{-2}$	$1.29 \times 10^{-2}$
	$s$	1.01	1.03	1.15
	$R^2$	0.9904	0.9916	0.9906

affinity. The density of the solution is extremely close to the density of the water (1 g/mL) at infinite dilution. The standard thermodynamic equilibrium constant ( $K_a^0$ ) of the adsorption process can be obtained from  $K_L$  using the activity other than concentration. To eliminate the unit of the equilibrium constant,  $K_a^0$  is given by:

$$K_a^0 = K_L \times 10^6 \text{ mg/L} \quad (5)$$

Thermodynamic parameters such as the changes in Gibbs free energy ( $\Delta G^0$ ), enthalpy ( $\Delta H^0$ ) and entropy ( $\Delta S^0$ ) were calculated using the following equations [23,24]:

$$\ln K_a^0 = -\frac{\Delta H^0}{RT} + \frac{\Delta S^0}{R} \quad (6)$$

$$\Delta G^0 = \Delta H^0 - T\Delta S^0 \quad (7)$$

$\Delta H^0$  and  $\Delta S^0$  were obtained from the slope and intercept of the plots of  $\ln K_a^0$  vs.  $1/T$  (Fig. 5), respectively. Table 4 shows the calculated values of the thermodynamic parameters. The positive values of  $\Delta H^0$  show that the adsorption process is more favorable at high temperature and the adsorption of MG on SSR is an endothermic process. The negative values of  $\Delta G^0$  show that the adsorption process is spontaneous. According to Jaycock and Parfitt's opinion, the change of free energy for physical adsorption is smaller than that for chemisorption [25]. The former is in the range of  $-20$  kJ/mol to  $0$ , and the latter is in the range of  $-80$  to  $-400$  kJ/mol. The free energy for the adsorption of MG on SSR is in the range of  $-20$  to  $-30$  kJ/mol, which means that the interaction between SSR and MG is a combination of chemisorption and physisorption. The positive value of  $\Delta S^0$  demonstrates adsorption occurs and randomness increases at the solid–liquid interface [26]. Mittal [27] studied the thermodynamics of the adsorption of MG on hen feather and came to the similar conclusion.

### 3.5. Effect of initial pH on the adsorption of MG on SSR

The pH of the working environment is a vital parameter for an adsorption system. To investigate the influence

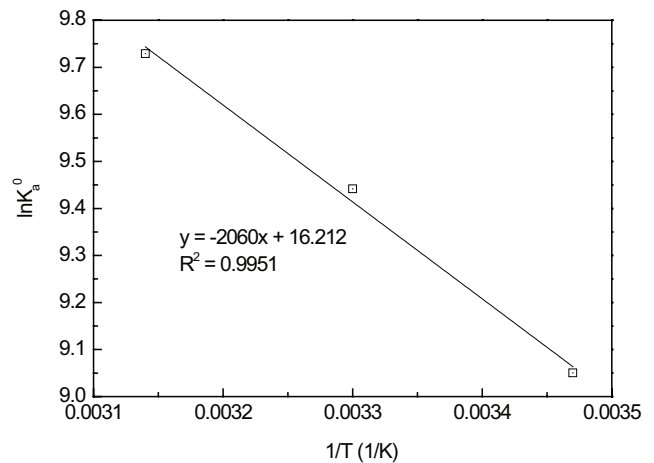


Fig. 5. The plot of  $\ln K_a^0$  vs.  $1/T$  for the adsorption of MG on SSR.

Table 4  
Thermodynamic parameters for the adsorption of MG on SSR

T (K)	$K_L$ (L/mg)	$\Delta G^0$ (kJ/mol)	$\Delta H^0$ (kJ/mol)	$\Delta S^0$ (J/(mol K))
288	$8.52 \times 10^{-3}$	-21.69		
303	$1.26 \times 10^{-2}$	-23.71	17.13	134.79
318	$1.68 \times 10^{-2}$	-25.73		

of pH on the adsorption capacity of MG, we conducted a series of experiments in the pH range from 2.0 to 10.0, and the result is shown in Fig. 6. With the increase of pH values from 2.0 to 10.0, the adsorption capacities first increase and then decrease. The optimal adsorption capacity, 50.6 mg/g, is achieved at pH 6.0. At the extreme pH of pH 2.0 and 10.0, the great reduction of adsorption capacity is caused by the change of color intensity. The reduction in the intensity in high pH is due to the alkaline fading of MG, while in low pH is due to the formation of  $MGH^{2+}$  species. [11] The phenomenon in the pH range of 4–8 may be explained by protonation and the mutual repulsion between the same charges. At low pH values, the sulfate groups of SSR exist in the form of  $-SO_3H$ , and they prevent the adsorption of MG onto SSR. At pH 6.0, the active sites become ionized and the cationic MG becomes adsorbed due to better valence forces between MG and SSR. When the values of pH exceed 6.0, the amino groups of MG become less positive and therefore the adsorption capacities decrease. Similar findings were reported for the adsorption of MG on oil palm trunk fibre [28] and magnesium phyllosilicate [29].

### 3.6. Reusability of SSR in dynamic adsorption

The reusability of an adsorbent is an important factor for its industrial application. As the filler of the adsorption column, high adsorption capacity and excellent desorption performance would reduce the usage cost of the adsorbent. The desorption experiments prove that adsorbed MG can be easily desorbed by using 1.0 mol/L HCl as desorption solution. The recyclability of SSR is shown in Fig. 7. From Fig. 7(A), we can know that the adsorbent becomes saturated with the

increasing of time which confirms the adsorbent has finite sites on the surface. However, after five cycles of adsorption and desorption process, the adsorption equilibrium time decreases from 150 min to 100 min. This can be explained by the decrease of the adsorption capacity. Fig. 7(B) shows that the desorption rate is rapid and the maximum concentration of desorption solution decreases. It suggests that not all the adsorbed MG molecules have been desorbed from the adsorbent [30]. The adsorption capacity decreases after five cycles, but SSR still shows a high adsorption capacity. The results indicate that SSR can be used as the filler of the adsorption column.

### 3.7. Comparative assessment of SSR as an adsorbent of MG

Table 5 shows the values of maximum adsorption capacity and the time to reach equilibrium for the adsorption of MG on different adsorbents. The maximum adsorption capacity is from the Langmuir isotherm fitting, and the time to reach

equilibrium is estimated from the effect of adsorption time on the adsorption capacities. Comparison of SSR with different adsorbents shows that SSR has a relatively great value of

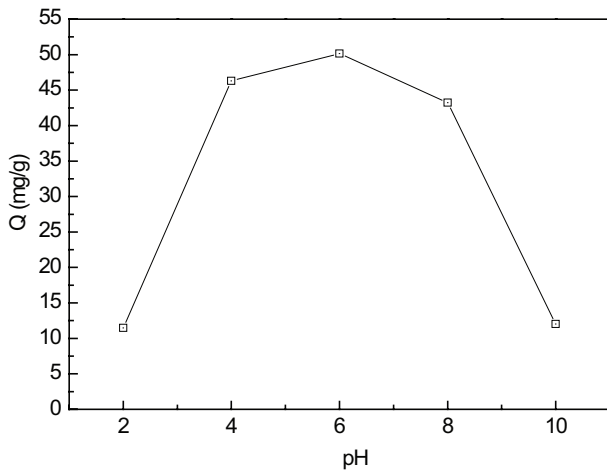


Fig. 6. Effect of pH on the adsorption capacities of MG at 288 K.

Table 5  
Comparison of SSR with other adsorbents of MG

Adsorbents	$Q_m$ (mg/g)	Time (min)	Reference
Clayey soil	78.57	60	[7]
Chitin hydrogels	33.57	1,680	[8]
Melamine/maleic anhydride sorbent	641.03	1,440	[9]
Carboxylate-functionalized multi-walled carbon nanotubes	11.73	10	[10]
Walnut shell	90.8	30	[11]
Bentonite	178.6	60	[21]
Chemically modified rice husk	17.98	20	[26]
Hen feathers	10.69	90	[27]
Oil palm trunk fiber	149.35	150	[28]
Aminopropyl-functionalized magnesium phyllosilicate	334.80	20–120	[29]
Granular composite hydrogel (AA-IA-APT5)	2,433	180	[30]
Peat of Brunei Darussalam	113.13	240	[31]
Chemically modified breadnut peel	353.0	>120	[32]
Chemical modification of <i>Artocarpus odoratissimus</i> skin	157.6	60	[33]
SSR	173.92	60	Present study

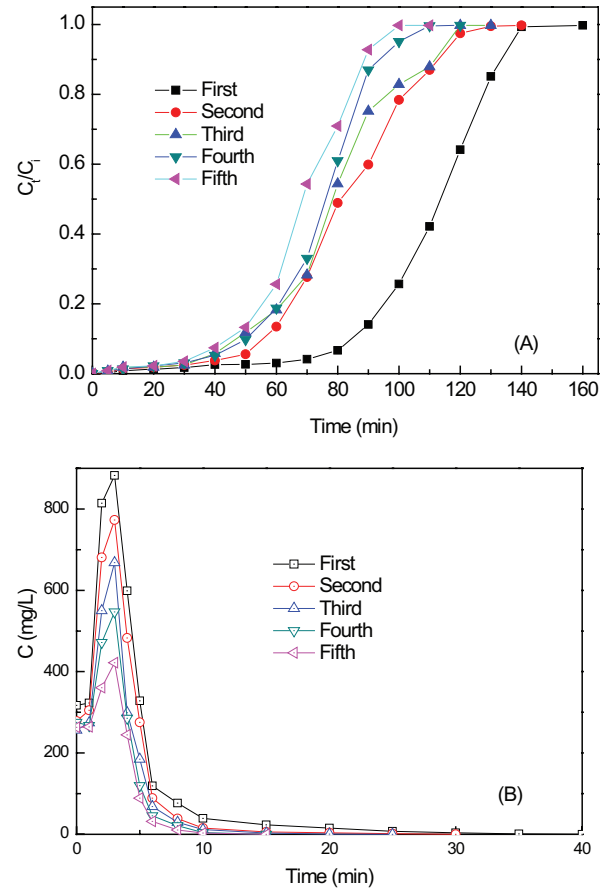


Fig. 7. Column adsorption curve (A) and column desorption curve (B) for the adsorption of MG on SSR at 288 K.

adsorption capacity and a relatively short adsorption time. In view of both the adsorption capacity and adsorption time, SSR is the optimum adsorbent of MG.

#### 4. Conclusions

The spherical SSR was prepared by an emulsion cross-linking method, and the adsorption performance of MG on SSR from aqueous solution was investigated. The adsorption reach equilibrium in about 60 min and the kinetic experimental data conform to the pseudo-first-order model. The adsorption equilibrium data are well described by the Langmuir isotherm model with a maximum adsorption capacity of 173.92 mg/g at 288 K. The results of adsorption thermodynamic studies indicate that the adsorption process is spontaneous and endothermic in nature. The adsorption capacities of MG on SSR first increase and then decrease with the pH increasing from 2.0 to 10.0, and the optimal adsorption performance is achieved at pH = 6.0. After five cycles of adsorption and desorption process, the adsorption capacity decreases, but SSR still exhibits excellent adsorption capacity. The spherical SSR is suitable as the filler of the adsorption column, and it has a promising potential for the removal of MG from waste effluent.

#### Acknowledgment

The authors acknowledge the National Natural Science Foundation of China (No. 21206066, 21171085, 21204035 and 21304043).

#### References

- [1] D.J. Alderman, Malachite green: a review, *J. Fish Dis.*, 8 (1985) 289–298.
- [2] S. Srivastava, R. Sinha, D. Roy, Toxicological effects of malachite green, *Aquat. Toxicol.*, 66 (2004) 319–329.
- [3] Z.H. Diao, X.R. Xu, F.M. Liu, Y.X. Sun, Z.W. Zhang, K.F. Sun, S.Z. Wang, H. Cheng, Photocatalytic degradation of malachite green by pyrite and its synergism with Cr(VI) reduction: performance and reaction mechanism, *Sep. Purif. Technol.*, 154 (2015) 168–175.
- [4] F.F. Wu, S. Wang, S.Y. Guo, H. Zhong, Adsorption of methylene blue by porous ceramics prepared from electrolytic manganese residues, *Desal. Wat. Treat.*, 57 (2016) 27627–27637.
- [5] L.N. Du, M. Zhao, G. Li, F.C. Xu, W.H. Chen, Y.H. Zhao, Biodegradation of malachite green by *Micrococcus* sp. strain BD15: biodegradation pathway and enzyme analysis, *Int. Biodeterior. Biodegrad.*, 78 (2013) 108–116.
- [6] N.A. Oladoja, Y.D. Aliu, Snail shell as coagulant aid in the alum precipitation of malachite green from aqua system, *J. Hazard. Mater.*, 164 (2009) 1496–1502.
- [7] P. Saha, S. Chowdhury, S. Gupta, I. Kumar, Insight into adsorption equilibrium, kinetics and thermodynamics of malachite green onto clayey soil of Indian origin, *Chem. Eng. J.*, 165 (2010) 874–882.
- [8] H. Tang, W. Zhou, L. Zhang, Adsorption isotherms and kinetics studies of malachite green on chitin hydrogels, *J. Hazard. Mater.*, 209 (2012) 218–225.
- [9] X. Rong, F. Qiu, J. Qin, J. Yan, H. Zhao, D. Yang, Removal of malachite green from the contaminated water using a water-soluble melamine/maleic anhydride sorbent, *J. Ind. Eng. Chem.*, 20 (2014) 3808–3814.
- [10] M. Rajabi, B. Mirza, K. Mahanpoor, M. Mirjalili, F. Najafi, O. Moradi, H. Sadegh, R. Shahryari-ghoshekandi, M. Asif, I. Tyagi, S. Agarwal, V.K. Gupta, Adsorption of malachite green from aqueous solution by carboxylate group functionalized multi-walled carbon nanotubes: determination of equilibrium and kinetics parameters, *J. Ind. Eng. Chem.*, 34 (2016) 130–138.
- [11] M.K. Dahri, M.R.R. Kooh, L.B.L. Lim, Water remediation using low cost adsorbent walnut shell for removal of malachite green: equilibrium, kinetics, thermodynamic and regeneration studies, *J. Environ. Chem. Eng.*, 2 (2014) 1434–1444.
- [12] G. Crini, Recent developments in polysaccharide-based materials used as adsorbents in wastewater treatment, *Prog. Polym. Sci.*, 30 (2005) 38–70.
- [13] L. Guo, G. Li, J. Liu, S. Ma, J. Zhang, Kinetic and equilibrium studies on adsorptive removal of toluidine blue by water-insoluble starch sulfate, *J. Chem. Eng. Data*, 56 (2011) 1875–1881.
- [14] S. Lagergren, About the theory of so-called adsorption of soluble substances, *K. Sven. Vetensk.akad. Handl.*, 24 (1898) 1–39.
- [15] Y.S. Ho, Adsorption of Heavy Metals from Waste Streams by Peat, PhD Thesis, University of Birmingham, Birmingham, 1995.
- [16] S. Wang, E. Ariyanto, Competitive adsorption of malachite green and Pb ions on natural zeolite, *J. Colloid Interface Sci.*, 314 (2007) 25–31.
- [17] I. Langmuir, The constitution and fundamental properties of solids and liquids. Part I. Solids, *J. Am. Chem. Soc.*, 38 (1916) 2221–2295.
- [18] H.M.F. Freundlich, Over the adsorption in solution, *J. Phys. Chem.*, 57 (1906) 385–470.
- [19] R. Sips, On the structure of a catalyst surface, *J. Chem. Phys.*, 16 (1948) 490–495.
- [20] L. Guo, C.M. Sun, G.Y. Li, C.P. Liu, C.N. Ji, Thermodynamics and kinetics of Zn (II) adsorption on crosslinked starch phosphates, *J. Hazard. Mater.*, 161 (2009) 510–515.
- [21] E. Bulut, M. Özacar, İ.A. Şengil, Adsorption of malachite green onto bentonite: equilibrium and kinetic studies and process design, *Microporous Mesoporous Mater.*, 115 (2008) 234–246.
- [22] S. Al-Asheh, F. Banat, R. Al-Omari, Z. Duvnjak, Predictions of binary sorption isotherms for the sorption of heavy metals by pine bark using single isotherm data, *Chemosphere*, 41 (2000) 659–665.
- [23] H.C. Schniepp, J.L. Li, M.J. McAllister, H. Sai, M. Herrera-Alonso, D.H. Adamson, R.K. Prud'homme, R. Car, D.A. Saville, I.A. Aksay, Functionalized single graphene sheets derived from splitting graphite oxide, *J. Phys. Chem. B*, 110 (2006) 8535–8539.
- [24] Z. Wang, J. Zhang, P. Chen, X. Zhou, Y. Yang, S. Wu, L. Niu, Y. Han, L. Wang, P. Chen, F. Boey, Q. Zhang, B. Liedberg, H. Zhang, Label-free, electrochemical detection of methicillin-resistant *Staphylococcus aureus* DNA with reduced graphene oxide-modified electrodes, *Biosens. Bioelectron.*, 26 (2011) 3881–3886.
- [25] M.J. Jaycock, G.D. Parfitt, *Chemistry of Interfaces*, Ellis Horwood Ltd., Onchester, 1981.
- [26] S. Chowdhury, R. Mishra, P. Saha, P. Kushwaha, Adsorption thermodynamics, kinetics and isosteric heat of adsorption of malachite green onto chemically modified rice husk, *Desalination*, 265 (2011) 159–168.
- [27] A. Mittal, Adsorption kinetics of removal of a toxic dye, Malachite Green, from wastewater by using hen feathers, *J. Hazard. Mater.*, 133 (2006) 196–202.
- [28] B.H. Hameed, M.I. El-Khaiary, Batch removal of Malachite Green from aqueous solutions by adsorption on oil palm trunk fibre: equilibrium isotherms and kinetic studies, *J. Hazard. Mater.*, 154 (2008) 237–244.
- [29] Y.C. Lee, E.J. Kim, J.W. Yang, H.J. Shin, Removal of malachite green by adsorption and precipitation using aminopropyl functionalized magnesium phyllosilicate, *J. Hazard. Mater.*, 192 (2011) 62–70.
- [30] Y. Zheng, Y. Zhu, A. Wang, Highly efficient and selective adsorption of malachite green onto granular composite hydrogel, *Chem. Eng. J.*, 257 (2014) 66–73.

- [31] C.H. Ing, T. Zehra, L.B.L. Lim, N. Priyantha, D.T.B. Tennakoon, Sorption characteristics of peat of Brunei Darussalam IV. Equilibrium, thermodynamics and kinetics of adsorption of methylene blue and malachite green dyes from aqueous solution, *Environ. Earth Sci.*, 72 (2014) 2263–2277.
- [32] H.I. Chieng, L.B.L. Lim, N. Priyantha, Enhancing adsorption capacity of toxic malachite green dye through chemically modified breadnut peel: equilibrium, thermodynamics, kinetics and regeneration studies, *Environ. Technol.*, 36 (2015) 86–97.
- [33] L.B.L. Lim, N. Priyantha, N.A.H. Mohamad Zaidi, U.A.N. Jamil, H.I. Chieng, T. Zehra, A. Liyandeniya, Chemical modification of *Artocarpus odoratissimus* skin for enhancement of their adsorption capacities toward toxic malachite green dye, *J. Mater. Environ. Sci.*, 7 (2016) 3211–3224.